Specific Mutagenesis of the Rieske Iron−Sulfur Protein in *Rhodobacter sphaeroides* Shows That both the Thermodynamic Gradient and the p*K* of the Oxidized Form Determine the Rate of Quinol Oxidation by the bc_1 Complex†

Mariana Guergova-Kuras,‡,§ Richard Kuras,§,|| Natalya Ugulava,|| Ivan Hadad,|| and Antony R. Crofts*,‡,||,⊥

Center for Biophysics and Computational Biology and Departments of Microbiology and Biochemistry, University of Illinois at Urbana−Champaign, 600 South Mathews Avenue, Urbana, Illinois 61801

Received October 27, 1999; Revised Manuscript Received April 3, 2000

ABSTRACT: In the Rieske iron−sulfur protein (ISP) of the ubiquinol:cytochrome c_2 oxidoreductase (bc_1 complex) of *Rhodobacter sphaeroides*, residue Tyr 156 is located close to the iron−sulfur cluster. Previous studies of the equivalent residue in both *Saccharomyces cerevisiae* [Denke, E., Merbitz-Zahradnik, T., Hatzfeld, O. M., Snyder, C. H., Link, T. A., and Trumpower, B. L. (1998) *J. Biol. Chem. 273*, 9085−9093] and *Paracoccus denitrificans* [Schroter, T., Hatzfeld, O. M., Gemeinhardt, S., Korn, M., Friedrich, T., Ludwig, B., and Link, T. A. (1998) *Eur. J. Biochem. 255*, 100−106] have indicated that mutations at this site can lead to modifications in the redox potential of the ISP. To study the effect of similar modifications on the thermodynamic behavior and kinetics of partial reactions of the bc_1 complex upon flash activation, we have constructed four mutant strains of *Rb. sphaeroides* where Tyr 156 was mutated to His, Leu, Phe, or Trp. The bc_1 complex was assembled and able to support photosynthetic growth in all mutants. Three substitutions (Leu, Phe, Trp) led to alteration of the midpoint potential (E_m) of the ISP and a slowing in rate of quinol oxidation, suggesting that electron transfer from quinol to the oxidized ISP controls the overall rate and that this step includes the high activation barrier. The Trp mutation led to an increase of ∼1 pH unit in the p*K* value of the oxidized ISP. The pH dependence of the rate of quinol oxidation in this mutant was also shifted up by ∼1 pH unit, showing the importance of the protonation state of the ISP for quinol oxidation. This provides support for a model in which the dissociated form of the oxidized ISP is required for formation of the enzyme−substrate complex [Ugulava, N., and Crofts, A. R. (1998) *FEBS Lett. 440*, 409−413].

The ubihydroquinone:cytochrome *c* oxidoreductase (E.C. 1.10.2.2) (bc_1 complex)[1] and the related b_6f complex of oxygenic photosynthesis provide the central elements of the major energy conversion pathways of the biosphere, catalyzing the transfer of electrons from a quinol to a small soluble protein such as cyt *c* by a modified Q-cycle (*1*−*3*). Electron transfer is linked to generation of a proton gradient across the membrane. The rate-limiting step in the mechanism is the oxidation of quinol at the Q_o site, where the first electron is transferred to a high-potential chain of single electron carriers (ISP, cyt c_1 and cyt *c*) and the second electron is transferred to a low-potential chain formed by cyt b_L and cyt b_H. Mechanistic aspects of this bifurcated reaction remain controversial (*4*−*10*). Brandt and Okun (*11*) have suggested that the activity of the bc_1 complex is controlled by two amino acid groups, with p*K* values of 6.5 and 9.2, which have to be dissociated and protonated, respectively, for maximal turnover. On the other hand, Ugulava and Crofts (*12*) have proposed that formation of the enzyme−substrate complex (ES complex) between quinol and the oxidized ISP, which precedes the quinol oxidation reaction, requires prior deprotonation of the ISP. In this scenario, the pH dependence of the rate of quinol oxidation reflects the availability of one of the substrates—the deprotonated ISP^{ox}. A similar model has been proposed by Snyder and Trumpower (*13*), in which the quinol at the Q_o site displaces a proton from one of the histidine ligands to the iron−sulfur cluster of the ISP.

The information obtained from the crystal structures of the bc_1 complexes (*10*, *14*, *15*) and their subunits (*16*, *17*) provides a context for understanding the mechanism at a molecular level and resolution of this controversy. Structures of isolated ISP from mitochondria and chloroplast complexes show that, although the sequence alignment of these two proteins shows a homology of only 28%, the overall structure is quite similar, and more strikingly the small domains containing the redox cofactor are almost superimposable. All residues that are completely conserved are located in this

† This work was supported by NIH Grant GM 35438.

* Address correspondence to this author at the Department of Biochemistry. Phone: (217) 333-2043. Fax: (217) 244-6615. E-mail: a-crofts@life.uiuc.edu.

‡ Center for Biophysics and Computational Biology.

§ Present address: Institut de Biologie Physico-Chimique, 13 rue P. et M. Curie, 75005 Paris, France.

|| Department of Microbiology.

⊥ Department of Biochemistry.

[1] Abbreviations: bc_1 complex, ubihydroquinone:cytochrome *c* (or c_2) oxidoreductase; b_H, higher potential cyt *b* heme; b_L, lower potential cyt *b* heme; cyt, cytochrome; ES complex, enzyme−substrate complex; ISP, iron−sulfur protein; ISP^{ox} and ISP^{red}, oxidized and reduced states of the iron−sulfur protein; Q, ubiquinone or quinone; QH_2, ubihydroquinone or quinol; QH^-, ubihydroquinone anion; Q_i site, quinone reducing site; Q_o site, quinol oxidizing site.

10.1021/bi992491+ CCC: $19.00
Published on Web 00/00/0000 PAGE EST: 8.8

domain, including Tyr 165 (bovine numbering). The hydroxyl side chain of this residue is located at hydrogen-bonding distance from the sulfhydryl group of Cys 139, which is a ligand to the Fe2 of the [2Fe-2S] cluster. Previous data showed that a Cys substitution for this Tyr in yeast leads to a complete loss of activity of the bc_1 complex, due to the nonassembly of the [2Fe-2S] cluster (*18*). On the basis of these data Iwata et al. (*16*) suggested an important structural role for this residue with possible implications for the assembly of the [2Fe-2S] cluster. A role in the electron transfer was also proposed by Carrell et al. (*17*), when they identified a nearly identical configuration in the chloroplast ISP. More recently, Denke et al. (*19*) and Schröter et al. (*20*) showed that mutations of the equivalent tyrosine in yeast and *Paracoccus denitrificans* could lead to modification of the ISP redox potential. However, the kinetic implications of these modifications were not investigated in detail, mainly because of the difficulties involved in studying such parameters in respiratory systems.

We have constructed four mutant strains of *Rhodobacter sphaeroides* in which the equivalent residue, Tyr 156, has been replaced by Phe, Trp, His, or Leu by site-directed mutagenesis. We have used these to investigate the effects of the protein environment on thermodynamic and spectral properties of the iron−sulfur cluster, assayed by EPR and CD spectroscopy. Kinetic spectrophotometry and flash excitation were used to investigate the effects on turnover of the Q_o site of the bc_1 complex in situ, by studying the partial reactions as a function of ambient redox potential and pH. Our results confirm that the rate of quinol oxidation is strongly dependent on the thermodynamic gradient of the reaction, as determined by the difference in redox midpotential (*13*, *19*). More importantly, we show that the p*K* value of the oxidized ISP controls the pH dependence of the rate of quinol oxidation.

EXPERIMENTAL PROCEDURES

Bacterial Strains and Culture Conditions. Escherichia coli strains were grown at 37 °C in LB medium supplemented with appropriate antibiotics, either ampicillin (100 μg/mL) or tetracycline (10 μg/mL). *Rb. sphaeroides* strains were grown in Sistrom medium at 30 °C either aerobically or photosynthetically. Strains containing the pRK415 derivative were maintained in the presence of 2 μg/mL tetracycline and 20 μg/mL kanamycin.

Construction of the Mutants. Syntheses of primers for PCR mutagenesis and sequencing of the mutant plasmids in order to confirm the mutations were performed at the Biotechnology Center of the University of Illinois. Site-directed mutagenesis was performed using plasmid pGBM as template with PCR methods as described in Kuras et al. (*21*). pGBM contains the whole *fbc* operon, cloned in pUC19, and is able to restore the WT properties of the BC17, a strain of *Rb. sphaeroides* bearing a deletion of the endogenous *fbc* operon (*22*). The *fbc* operon encodes the three major subunits of the bc_1 complex, the Rieske ISP (*fbc* F), the cyt *b* (*fbc* B), and the cyt c_1 (*fbc* C). Plasmid pGBM was first modified to introduce a six-histidine insert at the end of cyt *b* to facilitate rapid purification of the bc_1 complex (*23*), leading to plasmid pGBH6B.

Four mutations of codon 156 in the *fbc* F gene were generated using plasmid pGBH6B, to replace the WT Tyr with either Phe, His, Trp, or Leu. For each of the mutants an insert (i156*X*) containing the mutagenic codon was made using the following primers: (1) (p*X*) 5′ CGGGATC-*CCATGG*ATCGCAC[- - -]GACAGTGCCGGC 3′, where the mutagenic codon [- - -] corresponds to TTC for the Phe (*X* = F), CAC for the His (*X* = H), TGC for the Trp (*X* = W), and CTC for the Leu (*X* = L) substitution, and (2) (p2) 5′ GGAATTCATGCATCGCAAGCACGATGCCGGTG 3′.

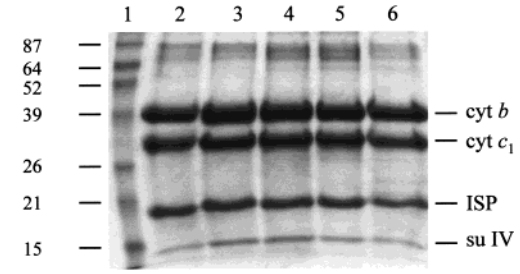

FIGURE 1: Coomassie staining of purified bc_1 complexes after SDS−PAGE. bc_1 complexes were purified from the WT (BH6 strain) (lane 2), Y156F (lane 3), Y156H (lane 4), Y156L (lane 5), and Y156W (lane 6) mutant strains using a his tag on the C-terminus of cyt *b*. Lane 1 is a molecular weight marker (BenchMark prestained protein ladder, Gibco BRL). A total of 25 μg of protein was loaded for each strain.

The PCR products were digested by *Eco*RI and *Bam*HI and cloned in pUC19. To introduce the mutation in the operon, an additional insert (i2) was generated using the following primers: (3) (p3) 5′ CGGGATCCTTCCTCGG-CAAACCGATCTTCATC 3′ and (4) (p4) 5′ GGAATT-*CCATGG*CAGGGGCAGAACCAGCCCCCG 3′.

The product was also digested by *Eco*RI and *Bam*HI and cloned in pUC19. Standard molecular biology techniques were used to fuse each of the inserts i156*X* with insert i2 using the *Nco*I site (shown in italics, underlined). The *Rsr*II and *Bst*BI restriction sites were then used to introduce the fusion products containing the mutation into pGBH6B. The *fbc* operons were subsequently subcloned into pRK415-1 and introduced into *Rb. sphaeroides* by conjugation with *E. coli* strain S17-1 (*22*).

Biochemical Methods. Purification of the bc_1 complex and polypeptide analysis were performed as previously described (*23*) from chromatophore preparations (*24*). For each lane in Figure 1, 25 μg of the purifed bc_1 complex, resuspended in 66 mM DTT, 66 mM Na_2CO_3, 2% (w/v) SDS, 10% (w/v) sucrose, and 3 mg/mL bromophenol blue, was loaded. The protein concentration was determined from the optical spectra of the reduced bc_1 complex (*25*). Polypeptides were visualized by Coomassie blue staining.

Biophysical Methods. All mutant strains were characterized through differential spectrophotometry to identify the three cytochrome components of the bc_1 complex; in addition, for all chromatophore preparations, the complement of redox centers was assayed by excitation using multiple flashes in the presence of antimycin and measurement at the wavelength pairs appropriate for individual components (*4*, *26*). The spectra and E_m values for the cytochrome components were the same within experimental error in all strains, and components were present in the same relative stoichiometry.

EPR spectra from the purified bc_1 complexes were obtained using a Varian E-112 X-band spectrometer equipped with an Air Products (Allentown, PA) variable temperature cryostat and a Varian TE_{102} mode cavity. The conditions used

Table 1

	EPR parameters				redox parameters				
	ascorbate reduced		in the presence of stigmatellin						
strain	g_y	g_x	g_y	g_x	E_m^{lim} [a] (mV)	ΔE_m^{lim} (mV)	rel rate[b]	pK_1	pK_2
WT	1.895	1.805	1.885	1.777	312 ± 5		100	7.6 ± 0.1	9.8 ± 0.4
Y156H	1.895	1.804	1.885	1.778	316 ± 7	4 ± 12	97	7.5 ± 0.1	10.4 ± 0.7
Y156F	1.897	1.804	1.885	1.783	256 ± 4	56 ± 9	58	7.5 ± 0.1	9.2 ± 0.2
Y156L	1.895	1.805	1.885	1.783	247 ± 5	65 ± 10	57	7.7 ± 0.1	11[c]
Y156W	1.890	1.820	1.879	1.804	198 ± 3	114 ± 8	7.2	8.5 ± 0.1	11[c]

[a] E_m^{lim} is the limiting value for E_m at pH ≪ pK_1. [b] The rate for wild type at pH 7 was 1330 mol·(mol of bc_1)$^{-1}$·s^{-1}. [c] These values were forced and lie outside the titration range. The curve was well fit by a single pK with the same value as pK_1.

were microwave frequency 9.05 GHz, microwave power 1 mW, modulation amplitude 12.5 G, and temperature 11 K.

CD spectroscopy was performed using a JASCO J-720 spectropolarimeter as described previously (*12*). The mutant bc_1 complexes were resuspended at 2 μM in the appropriate buffer in the presence of 0.01% dodecyl maltoside. Redox titrations were performed in a modified cylindrical cuvette as described in Ugulava and Crofts (*12*). Titration curves were obtained from the CD spectra by abstracting values at appropriate wavelengths (500 and 470 nm). The curves were fitted with a one-electron Nernst component using the built-in nonlinear least-squares-fitting algorithm of the data analysis program Origin 4.0 (Microcal Software, Inc., Northampton, MA).

Flash-induced kinetics were measured using a home-built kinetic spectrophotometer at a constant temperature (25 °C) as described previously (*4*). Chromatophores were suspended at about 0.4 μM RC in 100 mM KCl containing 50 mM appropriate buffer (see below) and with additions as indicated in the figures. The ambient redox potential in the cuvette was adjusted by adding small amounts of $K_3Fe(CN)_6$ or $Na_2S_2O_4$, and the suspension was kept anaerobic by a constant flow of argon gas. The following redox mediators were used in all kinetic experiments at a concentration of 10 μM each: DAD (E_m 245 mV), 1,2-naphthoquinone-4-sulfonic acid (E_m 217 mV), 1,2-naphthoquinone (E_m 145 mV), 1,4-naphthoquinone (E_m 60 mV), and *N*-methylphenazonium methosulfate (E_m 85 mV). Pyocyanine (E_m −60 mV) and Fe(III) NaEDTA (E_m 117 mV) were used at concentrations of 7 and 20 μM, respectively. Kinetics of cyt b_H reduction were followed at 561−569 nm (*26*). The rates were estimated either from the initial slope of cyt *b* reduction (in the presence of antimycin), normalized for the concentration of cyt *b* reduced after the first flash, or by deconvoluting the kinetics of cyt *b* reduction to a single-exponential component, assuming pseudo-first-order kinetics. The two methods gave similar results, although at pH ranges where the kinetics became fast, slight deviation from a single-exponential behavior was observed. The electrochromic band shift was measured from the absorbance change at 503 nm as described in Glaser and Crofts (*27*). Initial rates of the slow phase were determined from the difference kinetics without and with myxothiazole.

Buffers used both for the kinetic measurements and for the redox titrations of the ISP were MES for pH 5.0−6.5, MOPS to pH 7.5, EPPS to pH 8.5, and CHES to pH 10.

Molecular modeling was performed on a Silicon Graphics Indigo2 workstation using the program package Quanta (Molecular Simulations Inc., San Diego, CA). For the homology modeling of the ISP from *Rb. sphaeroides*, the Modeller module from the same package was used, with the coordinates for the soluble fragment of the bovine mitochondrial ISP (PDB file 1rie) as a structural template. An alignment of 20 bacterial and mitochondrial ISPs was first generated using ClustalW, and the database was further searched to obtain the best fits for the extra sequences characteristic for the purple bacteria. The sequence of *Rb. sphaeroides* corresponding to the soluble part was then used to generate the molecular model of the ISP. Since the program does not take into account the special configuration of cofactors, the coordinates for the [2Fe-2S] cluster were built from the mitochondrial structure. The conformations of the side chains of the two histidine ligands found after generation of the preliminary model were modified in order to adopt the geometry necessary for liganding the cluster. The conformity of the model to appropriate physicochemical parameters was verified by comparison with a database of structures with resolution of at least 2.0 Å (Procheck 3.4), and 98.2% of the residues were found in favored regions. The modeling of the Tyr 156 substitutes was based both on the structural model of the *Rb. sphaeroides* ISP and on the structure of the beef heart mitochondrial ISP. In each case, the structure of the backbone was fixed, and the best rotamers were calculated using modules in the Quanta package.

RESULTS

Choice of Mutations and Properties of the Mutant Strains. We have constructed four mutant strains of *Rb. sphaeroides* where Tyr 156 from the ISP was substituted by Phe, Trp, His, or Leu. The mutations were introduced in a context where cyt *b* contains a polyhistidine C-terminal extension (His_6 tag) to facilitate rapid purification of the bc_1 complex (*23*). All four strains were capable of growing photosynthetically, which indicates that none of these mutations led to an inactive bc_1 complex. The Y156H mutant showed the same growth rate as the WT (doubling time of 8 h), whereas growth of Y156F, Y156L, and Y156W was slightly slowed, with generation times of 10, 10, and 12 h, respectively. The purified bc_1 complex of the mutant strains showed all four subunits with a relative stoichiometry undistinguishable from that of the WT (Figure 1).

Properties of the [2Fe-2S] Cluster. The EPR spectra of the [2Fe-2S] center of ascorbate-reduced bc_1 complexes from Y156H, Y156F, and Y156L are similar to those of the WT with g_y and g_x bands at 1.895 and 1.800, respectively (Figure 2A and Table 1). By contrast, the signal from the Y156W mutant bc_1 complex showed a clear difference, particularly in the position of the g_x band that was shifted downfield to

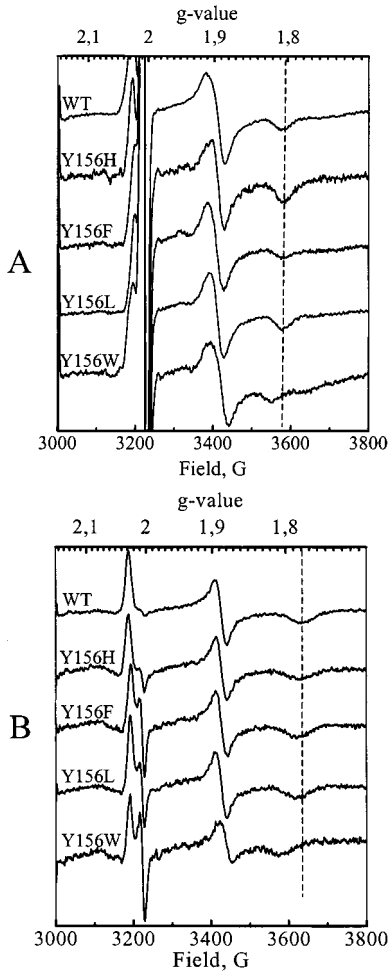

FIGURE 2: EPR spectra of the [2Fe-2S] cluster of the ISP from WT and mutant strains. (A) Purified bc_1 complexes (40 μM), resuspended in 50 mM MOPS, pH 7.0, 100 mM KCl, 0.01% (w/v) dodecyl maltoside, and 15 μg/mL phosphatidylcholine, were reduced with 1 mM sodium ascorbate for 5 min before freezing. (B) Same conditions as in (A) but in the presence of 60 μM stigmatellin. The dashed line shows the position of the g_x value in the WT.

1.82. The g_x band reflects an interaction between ISP^{red} and the Q_o site occupant, either quinone ($g_x = 1.80$) or inhibitor. Stigmatellin, an inhibitor that binds at the Q_o site and prevents the quinol oxidation, has been shown to modify the EPR spectra of the Rieske iron−sulfur cluster (*24*, *28*). In the presence of 60 μM stigmatellin we observed the characteristic shift of *g*-values in all of our mutants. Interestingly, although the Y156W strain presented a modified g_x value in its reduced state, it was still sensitive to the addition of stigmatellin to the same extent as the rest of the mutants (Table 1). Zhang et al. (*15*) have shown that, in the chicken mitochondrial complex, stigmatellin contacts the ISP, modeled as a hydrogen bond through one of the His ligands (His 161, bovine numbering) of the metal center. It has been suggested that such a complex might mimic a reaction complex, either a semiquinone−ISP intermediate formed during the quinol oxidation (*9*) or the ES complex between quinol and the oxidized ISP formed before quinol oxidation (*12*, *15*, *29*). Since all complexes showed a g_x band of the EPR spectrum when either quinone or stigmatellin occupied the Q_o site, it seems likely that, in the mutant complexes, the interactions between the reduced ISP and the Q_o site occupant were not seriously modified. The differences in the EPR spectra of strain Y156W probably originate from changes in the local environment of the cluster (see Discussion).

The redox properties of the Rieske iron−sulfur center in the mutant strains were investigated by CD spectroscopy. It has been shown that the Rieske ISP has a typical CD spectrum with a broad negative band around 500 nm in its reduced state (*30*, *31*). This property has been used to probe both the redox potential of this protein and its pH dependence (*12*, *32*). Redox titrations of the purified bc_1 complexes from the mutant strains were performed at different pH values in the range from 5.0 to 10.5. All of the titration curves could be fitted to a Nernst equation with $n = 1$. The midpoint potentials determined at each pH for the different mutants were plotted in Figure 3. It was previously observed that, in the pH range used for our study, the E_m value of the ISP from *Rb. sphaeroides* is constant below pH 7 and decreases above this point in both the purified bc_1 complex and in membranes (*12*, *33*). The data were fitted using either one or two p*K* values with $pK_1 \sim 7.6$ and $pK_2 \sim 9.8$. These values are similar to those found for beef heart mitochondria (*32*). The results of the deconvolution using two p*K* values are summarized in Table 1, and the fits with these parameters are shown in Figure 3. Several observations on the effect of the mutations on the redox potential of the ISP are noteworthy:

(1) The His substitution did not significantly alter the E_m^{lim} value of the ISP, whereas the three other mutations led to a decrease in the E_m^{lim} of either ~60 mV (Y156F and Y156L) or 100 mV (Y156W).

(2) Neither pK_1 nor pK_2 was markedly altered by replacement with either Phe or His. In contrast, the Y156W mutation introduced an increase in the value of pK_1, which was shifted by ~1 pH unit to 8.5 ± 0.1. The data suggest that, if a second p*K* is assumed, its value might have been altered in both Y156W and Y156L mutants. However, we should note that the pH dependencies for all strains could be fit quite well with a single p*K* and, for these two mutants, could be fit better with only one p*K* value of 8.5 ± 0.1 or 7.7 ± 0.1, respectively. When fitted with two p*K* values, the second p*K* had to be fixed at higher than 11 in order to obtain the same quality of the fit and thus was beyond the range of the titration data.

Electron Transfer Properties of the bc_1 Complex. Modifications in the midpoint potential of the ISP have been shown to alter the activity of the bc_1 complex (*18*−*20*, *34*). This is consistent with the hypothesis that the quinol oxidation by the ISP contains the rate-limiting partial reaction (*13*, *35*). The flash-induced kinetics of quinol oxidation in the four mutants and the WT, measured at pH 7.5 through cyt b_H reduction in the presence of the Q_i site inhibitor antimycin, are shown in Figure 4A. The decrease in the E_m of the ISP in mutant strains was associated with a decrease in the rate of quinol oxidation, but the correlation was clearly not linear. Indeed, a decrease of 60 mV (Y156F and Y156L) led to an ~1.7-fold decrease in the rate constant whereas an additional 40 mV drop in mutant Y156W induced a 14-fold loss of activity (96 s^{-1} as compared to 1330 s^{-1} for the WT). Also noteworthy is the longer lag before onset of the maximal rate seen in the Y156W strain; a similar lag is seen in wild type at lower pH (*7*). Since the p*K* value of the ISP in this

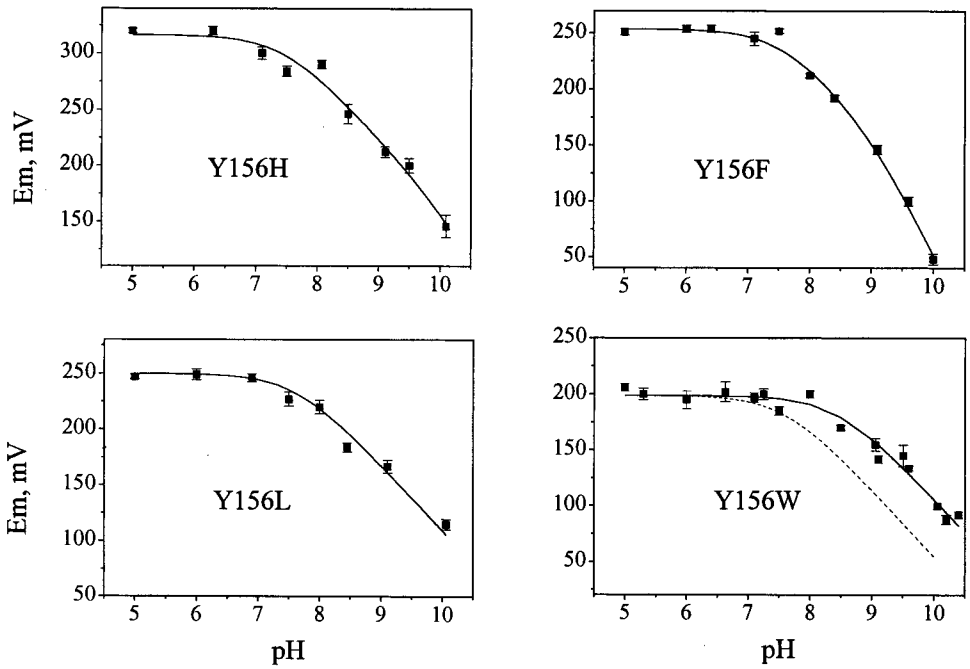

FIGURE 3: pH dependence of the midpoint potential of the mutant ISPs. The solid lines represent the fits with the parameters summarized in Table 1. The dashed line is a simulated fit with a pK_1 of 7.6 for the Y156W mutant.

mutant is also modified, and this could contribute to the rate constant by decreasing the concentration of deprotonated ISP^{ox}, we have extended our study to include the protonation state of the ISP by following the kinetics of quinol oxidation at different pHs. The pH dependencies of the quinol oxidation in the mutant strains and the WT are shown in Figure 4B. The kinetics of cyt b_H reduction in the presence of antimycin were measured at different pH values at 25 °C. In all experiments, the initial relative concentration of ubiquinol was set to ~30% of the whole quinone pool by adjusting the redox potential of the reaction mixture. It has previously been shown that, with this relative amount of quinol, the rate of cyt b_H reduction approaches a maximum and reflects the rate-limiting step, which corresponds to the oxidation of a quinol at the Q_o site (*4*, *26*). When the concentration of quinol was adjusted in this way, cyt b_L and cyt b_H were both oxidized prior to the flash over the pH range 5.5−8.0, and a saturating flash introduced the same concentration of oxidized cyt c_2 to the complex, so that the initial concentrations of the reactants of the overall reaction were the same immediately after excitation at each pH. In this pH range we observed that the rate of quinol oxidation in the mutants Y156H, Y156F, and Y156L was strongly pH dependent, increasing up to a maximum at pH ~7.5, as previously observed in the WT (Figure 4B and ref *7*). It should be noted that the amplitude of the absorbance change due to heme b_H was similar in all strains when measured over an appropriate time scale. Interestingly, mutant Y156W showed a different pH dependence of the rate. There was practically no dependence on pH over the range 5.5−7.5, but a substantial increase between pH 7.5 and pH 8.0, suggesting that the maximum rate could be out of the pH range of these experiments (Figure 4B, open diamonds). The kinetics of quinol oxidation in this mutant in the alkaline region were measured using the electrogenic reactions of the bc_1 complex. Since the midpoint potential of cyt b_H is pH independent above the pK at ~7.8, while the quinone pool continues to show a pH dependence up to much higher pH, for experiments above this pH, redox conditions that provide the same initial concentration of quinol will also poise cyt b_H partly in its reduced form prior to the flash. Measurement of the initial rate of reduction of cyt b_H could not therefore be used to estimate the rate of quinol oxidation at pH >8.5. The electrogenic events accompanying the uninhibited turnover of the complex can be assayed through the slow phase of the carotenoid electrochromic band shift at 503 nm (*4*, *7*, *27*). The initial rate of the slow phase is determined by the rate-limiting step of the overall reaction, which is that of the Q_o site, and is therefore an indirect measure of the rate of quinol oxidation (*2*, *4*, *7*, *26*, *27*). Using these two alternative approaches, Hong et al. (*7*) were recently able to measure the activation barrier for this reaction as a function of pH, thus confirming the complementarity of the two methods. The pH dependence of the rate of the slow phase in the Y156W mutant confirms the increase in the pH range 7.5−8.0 observed by the cyt *b* reduction (Figure 4B). The maximal rate is attained only at pH ~8.9, which is significantly higher than the optimal pH for the WT and could reflect the shift of the pK value of ISP^{ox} in this mutant (see Discussion).

DISCUSSION

All mutations so far reported to change the redox potential of the ISP are within 7 Å of the center of the cluster. From the four substitutions of Tyr 156 reported in the present work, we found that three of them, Tyr to Leu, Phe, or Trp, decreased the midpoint potential of the cluster as summarized in Table 1. On the basis of sequence alignment, residue Tyr 156 from the *Rb. sphaeroides* ISP corresponds to residue Tyr 165 in the sequence of the beef mitochondrial ISP and to Tyr 132 in the ISP of spinach chloroplast. In the crystal structures of the proteins from both organisms, the equivalent Tyr is one of those lying close to the metal cluster (*16*, *17*). Moreover, the hydroxyl group of the side chain was found

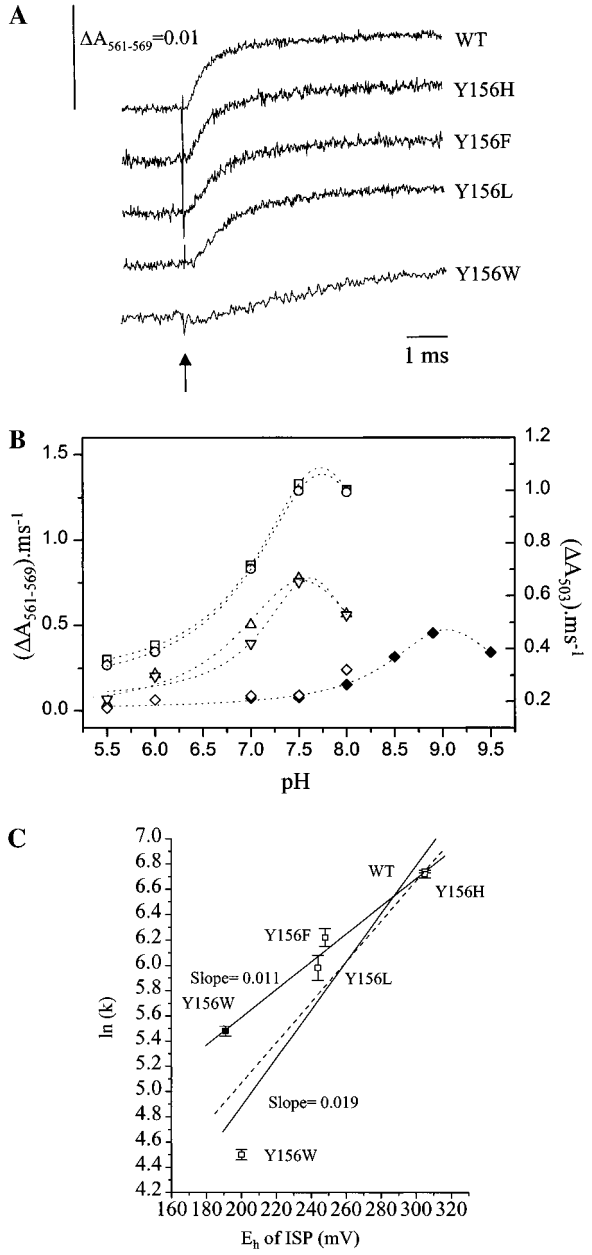

FIGURE 4: Kinetics of electron transfer in the mutant strains. (A) Flash-induced kinetics of cyt b_H reduction at pH 7.5. Chromatophores were resuspended in 50 mM MOPS (pH 7.5), 100 mM KCl, and redox mediators as indicated in Experimental Procedures; 5 μM valinomycin, 2 μg/mL gramicidin, and 5 μM antimycin were also present. The ambient potential was poised at 70 mV at 25 °C. Traces were normalized for the total amplitude of cyt b_H reduction. (B) pH dependence of the rate of quinol oxidation in the WT (□), Y156H (○), Y156F (△), Y156L (▽), and Y156W (◇) mutant strains. Open symbols: rate determined from cyt b_H reduction in the presence of 5 μM antimycin. Closed symbols: rate determined from the slow myxothiazole-sensitive phase of the kinetics of the carotenoid band shift. (C) Dependence of the rate of quinol oxidation on E_m of ISP. The rates determined from cyt b_H reduction at pH 7 for all mutant strains are shown as open symbols; the rate for Y156W at pH 8 is added as a closed symbol. The E_m values at a specific pH were taken from the simulation curves of Figure 3. The standard deviation at each rate is shown with bars. Slopes are shown for the best fit using either data point for the Y156W strain. The dashed line shows the slope of 0.016 mV^{-1}, expected from a Marcus treatment of the model discussed in ref *7*. The curvature expected from a Marcus curve is not appreciable over this range of ΔE.

at hydrogen-bonding distance from the sulfhydryl liganding group of Cys 139 (bovine, C129 in *Rb. sphaeroides* numbering) in both the mitochondrial and the chloroplast ISP. Since structures of these two ISPs, which are distantly related and share only 28% homology, show an almost identical organization of their cluster binding domain, it seemed likely that the purple bacterial ISP, for which the homology to the mitochondrial ISP is 57%, would also show the same structural similarity. A molecular model of the ISP from *Rb. sphaeroides* based on homology modeling with the mitochondrial ISP showed no differences in the small (cluster binding) domain and only two additional loops in the large domain as compared to the mitochondrial ISP (Figure 5). In our molecular model, Tyr 156 (*Rb. sphaeroides* numbering) is located in a similar, hydrogen-bonding distance from Cys 129.

The EPR spectra of the ISP in the mutants indicate that the Phe, Leu, and His substitutions introduce rather small structural perturbations. Indeed, the g_x band, which reflects the interactions of the ISP with either the quinone or stigmatellin occupant of the Q_o site (Figure 2), and the CD spectra (not shown) measured in these mutants were identical to those of the WT. The change in midpoint potential of the ISP in Y156L and Y156F could well reflect the inability of Leu and Phe side chains to participate in hydrogen bonding. In both mutant strains, we observed a decrease of the ISP midpoint potential to ~250 mV. Similar results were obtained in yeast and *P. denitrificans* where the substitution of Tyr to Phe showed a decrease in the midpoint potential of the ISP by 65 and 44 mV, respectively (*19*, *20*). Interestingly, the midpoint potential of the ISP was not altered by the substitution to His. This result might seem surprising since in the model structure the mobile hydrogen from the imidazole ring appears to be too far away from Cys 129, the sulfhydryl ligand, to allow the formation of an H-bond. However, it should be noted that the hydrogen bond network around the metal center is not as rigid as originally indicated (*16*); in the structures of the ISP reported by Iwata et al. (*10*) for the bovine bc_1 complex in $P6_5$ and $P6_522$ crystal forms, the distance between the hydroxyl group of Tyr 165 and the sulfhydryl liganding group of Cys 139 (bovine numbering) is different. The distance increased to 4 Å when the ISP was close to cyt *b* (*Int* position, found in one monomer in $P6_5$ crystals) as compared to 2.9 Å, when the ISP was close to cyt c_1 (in $P6_522$ crystals) or in the soluble fragment (*16*). Thus, the Tyr is too far away from the Cys in the *Int* position to form a hydrogen bond. Interestingly, Iwata et al. (*10*) observed an alternative H-bond network between the cluster binding and the base region in the *Int* conformation as compared to the cyt c_1 conformation or the structure of the soluble fragment. We could interpret these differences in several ways. It seems possible that even if the His substituent does not allow the same H-bonding pattern as the native structure, its imidazole ring might still allow participation in a H-bond network, either directly or through a bridging H_2O molecule. Alternatively, it may be that formation of a H-bond is not the critical factor in determining the redox potential but that polarity, contributed either by the imidazole ring or by the tyrosine −OH, is important.

For both the leucine and histidine mutants, our results contrast strongly with those obtained with the equivalent substitutions in yeast, where it was reported that both

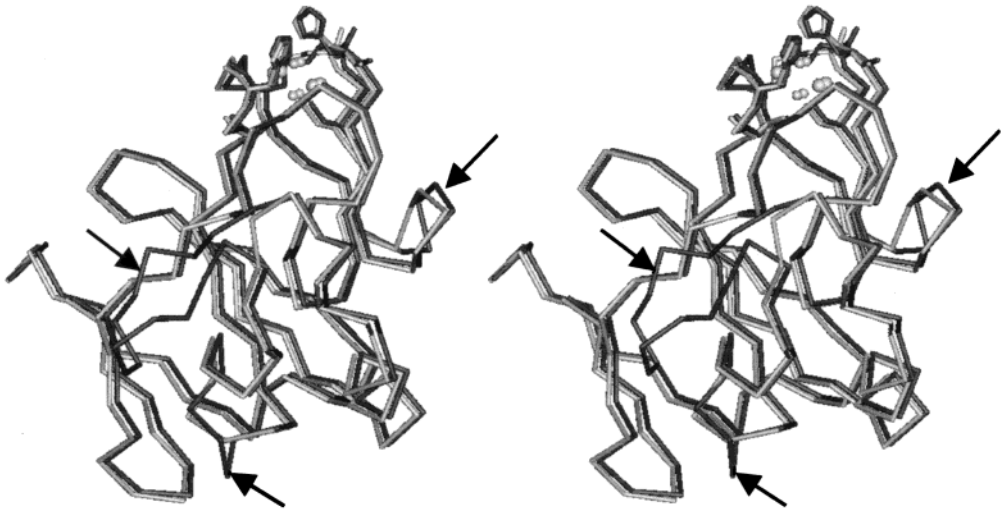

FIGURE 5: Comparison of the molecular model of the ISP from *Rb. sphaeroides* to the soluble fragment of the bovine mitochondrial ISP (PDB file, 1rie). Stereoview of the protein backbone, shown as a Cα trace, and the [2Fe-2S] cluster, shown as a space-filling model. The two structures were superimposed and subsequently translated apart for better viewing. The insertions and extra loops in the bacterial structure are indicated with arrows.

mutations prevented the accumulation of the ISP and thus impaired the activity of the bc_1 complex. Additionally, although the Y156W mutant protein was accumulated in both the yeast and bacterial systems, the yeast protein was reported to be less stable. Since none of our mutants showed any indication of an unstable ISP subunit, we have been able to better characterize these strains, taking advantage of the stability in *Rb. sphaeroides*. When estimated from the ratio RC/bc_1 complex, determined from flash-induced kinetics, the amount of functional bc_1 complex in our mutant strains appeared similar to that of the WT (not shown), and the amplitudes of the kinetic traces for all cytochromes, and EPR spectra, were similar. Moreover, the subunit composition and purification parameters for the mutant bc_1 complexes were similar to those of the WT, leading in every case to a purified bc_1 complex in which the four subunits were present with a similar stoichiometric ratio (Figure 1). Taken together, these results argue against the presence of partially assembled bc_1 subcomplexes that lack the ISP protein in any of our mutant strains.

In contrast to the other substitutions, the EPR spectra of the ISP in the Y156W mutant appeared substantially modified as compared to that of the WT, although the strain retained the characteristic Rieske-type signal and its sensitivity to stigmatellin or interaction with quinone (Figure 2). When the Trp substitution was modeled in the structure of the soluble ISP, the side chain, even in the optimal position, formed close contacts with neighboring residues. Interestingly, the best rotamer of the Trp showed only two close contacts, both with Ser 163 (bovine numbering), a hydrogen bond donor to the [2Fe-2S] cluster. Mutations of Ser 163 have previously been shown to decrease the midpoint potential of the ISP by 130 mV (*19*). It is therefore possible that the structural rearrangements needed to accommodate the Trp residue in the Y156W mutant also perturbed the hydrogen bonding of Ser 154 (*Rb. sphaeroides* numbering) and led to the substantially lower midpoint potential of Y156W as compared to Y156F and Y156L. Molecular modeling of the latter two substitutions showed no close contacts with the neighboring residues.

The pH dependence of the ISP redox potential, first observed in chromatophores from *Rb. sphaeroides* and mitochondrial membranes by Prince and Dutton (*33*), was fitted with a p*K* value of 8.0 for the oxidized ISP. A similar pH dependence of the ISP redox potential has been reported in numerous other systems (*12*, *32*, *33*, *36*, *41*−*47*), although some authors have shown that the pH dependence of the ISP redox potential could also be fitted with two p*K* values. Attribution of the p*K* on the oxidized form to dissociation of a histidine comes from detailed spectroscopic studies. Changes in the Mossbauer spectrum of the ISP with pH (*36*) were interpreted as showing that one of the histidine ligands was responsible for the pH dependence of the E_m of the Rieske ISP. This was later supported by resonance Raman studies of the Rieske-type ISP from *Thermus thermophilus*, in which the spectral transitions sensitive to pH were identified as Fe(III)−N(His) stretching motions, showing that between pH 7.3 and pH 10.1 the imidazole undergoes deprotonation (*37*). The structures of the bovine and chicken mitochondrial bc_1 complexes showed that His 161 (bovine numbering) forms a hydrogen bond with the propionate of the heme *c* in cyt c_1 (*10*, *15*) or stigmatellin bound in the Q_o site (*15*) depending on the conformational state of the complex. The identification of His 161 as the residue controlling the pH dependence of the E_m of the ISP is generally well accepted (*12*, *16*, *32*, *35*). The value of pK_1 was altered substantially in the Y156W mutant, showing an increase of almost 1 pH unit. As pK_1 was only slightly or not altered by the Phe, His, or Leu substitutions, the change in the pK_1 observed in the Y156W mutant could not be attributed simply to the replacement of Tyr 156, or loss of the H-bond, and would have to reflect more general structural perturbations in the overall cluster binding region, perhaps through the steric interaction with Ser 154, as discussed above.

The decrease of the E_m value of the ISP in the mutant strains led to a decrease in the activity of the bc_1 complex (Figure 4C). Such a correlation was already observed in mutants of yeast (*19*, *38*), *Rhodobacter* (*34*, *39*), and *P. denitrificans* (*20*). In most cases it is difficult to correlate

directly the change in the E_m with the decrease in activity of the complex since the mutation may introduce additional perturbations that can obscure the effect of the E_m change. For example, a decrease of 20 or 104 mV in the E_m value in mutants of *Rb. capsulatus* ISP where Leu 136 (L142 bovine numbering) was changed respectively to either His or Gly led to an identical decrease (96%) in the activity of the bc_1 complex which was attributed to a perturbed docking interface between the ISP and cyt *b* in the region of the Q_o site (*39*). Even so, studies of ISP mutants showing a shifted E_m value can provide useful insights about the mechanism of quinol oxidation. The E_m value determines the driving force for the electron transfer reaction (through the contribution to $\Delta G°'$) and also the occupancy of the intermediate semiquinone state. The activation barrier for the overall two-electron reaction of quinol oxidation was shown to be ~45−65 kJ·mol^{-1} (*7*, *40*), but the location of the activated step has been controversial. Crofts and Wang (*4*) suggested that this would be in the first electron transfer and had speculated that the resulting semiquinone might represent the transition state. Kim et al. (*51*) have suggested that the two electron transfer reactions occur "simultaneously", implying a similar mechanism. In either case, assuming that the E_m of the QH_2/SQ couple was unaffected by mutation, the value for ΔG^{act} would be modified in direct proportion to the change in E_m of the ISP. If this were so, then, from a simplistic Arrhenius approach, a slope closer to F/RT (or 0.039 mV^{-1}) would be expected in the plot of Figure 4C. The weaker slope observed makes these mechanisms seem unlikely. Two of the slopes in Figure 4C are least squares linear fits to the data, one obtained using the data point for the Y156W mutant measured at pH 7.0 (with slope 0.0179 mV^{-1}) and the other (0.011 mV^{-1}) using the rate measured at pH 8.0, to allow for the lower concentration of the dissociated form of ISP^{ox} expected from the increased pK_1 in this strain. Both slopes are in the range expected if the overall rate was determined by the rate of the first electron transfer, using appropriate parameters from Marcus theory (~0.011−0.016 mV^{-1}, depending on model and assumptions; *7*, *48*−*50*), as shown by the third slope (dashed line). A more detailed discussion in terms of Marcus theory for electron transfer is given in a separate paper (*7*). Additional ambiguity in interpreting the effect of the p*K* change is introduced by the possibility that the driving forces for electron transfer and proton transfer might contribute separately in determining the rate (*50*; see below). Because the driving force for proton transfer is determined by the p*K* values of the groups contributing to the H-bond through which transfer occurs, the change in p*K* of the bridging histidine would be expected to change this contribution.

Since the pH profile for rate of reaction was shifted up to reflect the higher p*K*, our results with the Y156W mutant provide support for the suggestion that the enzyme−substrate complex involves binding of the dissociated oxidized ISP and that the ISP acts as a hydrogen carrier in the bc_1 complex (*7*, *12*, *13*, *35*, *40*). A possible role of the ISP as a proton carrier in b_6f complexes has been discussed by Carrell et al. (*17*) in the context of a buried water channel in cyt *f* (*52*) and a possible role in H^+ transfer from the Q_o site. It is therefore of interest to consider if a mechanism similar to that proposed by Ugulava and Crofts (*12*) might also control the rate of electron flow in the chloroplast b_6f complex. In chloroplasts, the ΔpH component of the proton gradient is thought to contribute a larger fraction and to play an important role in regulation. Some discrepancy exists between values for the p*K* on the oxidized form of the chloroplasts ISP. Earlier studies of the pH dependence of the redox potential in the chloroplast ISP indicated a p*K* value similar to that found for mitochondria (*41*), but more recently, Zhang et al. (*42*) found a lower p*K* value of 6.5 for the isolated chloroplast ISP fragment. This latter value is more in line with the pH dependence of the rate of plastoquinol oxidation by the b_6f complex. Hope et al. (*53*) showed a pK_1 of 6.1 for quinol oxidation. Similar results for the rate of cyt *f* rereduction in intact chloroplasts, which reached a maximum at pH 6.5, were reported by Nishio and Witmarsh (*54*). From these results we would suggest that the rate of plastoquinol oxidation in chloroplasts might also be determined by the availability of the dissociated oxidized ISP for formation of the ES complex.

This is the first report of a p*K* shift induced by mutagenesis in the Rieske protein and has profound implications not only for the mechanism of the bc_1 complex but also for the family of related proteins in which a similar 2Fe-2S cluster is found, but with different redox properties. For the mechanism of quinol oxidation, it seems possible that the first electron transfer is proton coupled and occurs through an ETPT mechanism [as defined by Cukier and Nocera (*50*)]. The slow rate for coupled electron and proton transfer through the short distance of a bridging H-bond and the high value of λ observed experimentally (*7*) are diagnostic of such a reaction. If so, this represents the first well-characterized reaction of this type in a biochemical system. In the theoretical treatment these authors suggest (*50*), the contributions from proton transfer and electron transfer to the driving force for the reaction, appearing in the Franck−Condon term of the Marcus equation, are separated. The former (proton transfer) contribution can be determined from the p*K* values of the groups contributing to the H-bond through which transfer occurs. The determination of the p*K* value for ISP^{ox} and its change in a mutant strain therefore represent the first step toward a deeper understanding of the mechanism, since the approach opens the possibility of studying the effect on reaction rate of a change in the driving force for the proton transfer. In the absence of additional data points, a more complete treatment in the present paper seems premature. However, we anticipate that strains with different p*K* values might be obtained through additional mutagenesis and look forward to a more complete treatment in that context.

ACKNOWLEDGMENT

We are grateful to Dr. Thomas Link for providing coordinates of the ISP fragment before publication. We thank Dr. Yao-Min Xia and the Illinois EPR Research Center for help with the EPR measurements and Dr. W. Mantulin and the Laboratory for Fluorescence Dynamics, Uuiversity of Illinois, for help with CD spectroscopy.

REFERENCES

1. Mitchell, P. (1976) *J. Theor. Biol. 62*, 327−367.
2. Crofts, A. R. (1985) in *The Enzymes of Biological Membranes* (Martonosi, A. N., Ed.) Vol. 4, pp 347−382, Plenum Publishing Corp., New York.

3. Brandt, U., and Trumpower, B. (1994) *Crit. Rev. Biochem. Mol. Biol. 29*, 165−197.
4. Crofts, A. R., and Wang, Z. (1989) *Photosynth. Res. 22*, 69−87.
5. Ding, H., Robertson, D. E., Daldal, F., and Dutton, P. L. (1992) *Biochemistry 31*, 3144−3158.
6. Jünemann, S., Heathcote, P., and Rich, P. R. (1998) *J. Biol. Chem. 273*, 21603-21607.
7. Hong, S., Ugulava, N., Guergova-Kuras, M., and Crofts, A. R. (1999) *J. Biol. Chem. 274*, 33931−33944.
8. Brandt, U. (1996) *FEBS Lett. 387*, 1−6.
9. Link, T. A. (1997) *FEBS Lett. 412*, 257−264.
10. Iwata, S., Lee, J. W., Okada, K., Lee, J. K., Iwata, M., Rasmussen, B., Link, T. A., Ramaswamy, S., and Jap, B. K. (1998) *Science 281*, 64−71.
11. Brandt, U., and Okun, J. G. (1997) *Biochemistry 36*, 11234−11240.
12. Ugulava, N. B., and Crofts, A. R. (1998) *FEBS Lett. 440*, 409−413.
13. Snyder, C., and Trumpower, B. L. (1998) *Biochim. Biophys. Acta 1365*, 125−134.
14. Xia, D., Yu, C.-A., Kim, H., Xia, J.-Z., Kachurin, A., Zhang, L., Yu, L., and Deisenhofer, J. (1997) *Science 277*, 60−66.
15. Zhang, Z., Huang, L., Shulmeister, V. M., Chi, Y. I., Kim, K. K., Hung, L. W., Crofts, A. R., Berry, E. A., and Kim, S. H. (1998) *Nature 392*, 677−684.
16. Iwata, S., Saynovits, M., Link, T. A., and Michel, H. (1996) *Structure 4*, 567−579.
17. Carrell, C. J., Zhang, H., Cramer, W. A., and Smith, J. L. (1997) *Structure 5*, 1613−1625.
18. Graham, L. A., Brandt, U., Sargent, J. S., and Trumpower, B. L. (1993) *J. Bioenerg. Biomembr. 3*, 245−257.
19. Denke, E., Merbitz-Zahradnik, T., Hatzfeld, O. M., Snyder, C. H., Link, T. A., and Trumpower, B. L. (1998) *J. Biol. Chem. 273*, 9085−9093.
20. Schroter, T., Hatzfeld, O. M., Gemeinhardt, S., Korn, M., Friedrich, T., Ludwig, B., and Link, T. A. (1998) *Eur. J. Biochem. 255*, 100−106.
21. Kuras, R., Guergova-Kuras, M., and Crofts, A. R. (1998) *Biochemistry 37*, 16280−16288.
22. Yun, C. H., Beci, R., Crofts, A. R., Kaplan, S., and Gennis, R. B. (1990) *Eur. J. Biochem. 194*, 399−411.
23. Guergova-Kuras, M., Salcedo-Hernandez, R., Bechmann, G., Kuras, R., Gennis, R., and Crofts, A. R. (1999) *Protein Expression Purif. 15*, 370−380.
24. Bowyer, J. R., Dutton, P. L., Prince, R. C., and Crofts, A. R. (1980) *Biochim. Biophys. Acta 592*, 435−460.
25. Vanneste, W. H. (1966) *Biochim. Biophys. Acta 113*, 175−178.
26. Crofts, A. R., Meinhardt, S. W., Jones, K. R., and Snozzi, M. (1983) *Biochim. Biophys. Acta 723*, 202−218.
27. Glaser, E. G., and Crofts, A. R. (1984) *Biochim. Biophys. Acta 766*, 322−333.
28. Von Jagow, G., and Ohnishi, T. (1985) *FEBS Lett. 185*, 311−315.
29. Crofts, A. R., Barquera, B., Gennis, R. B., Kuras, R., Guergova-Kuras, M., and Berry, E. A. (1999) in *The Phototrophic Prokaryotes* (Peschek, G. A., Loeffelhardt, W., and Schmetterer, G., Eds.) pp 229−239, Plenum Publishing Corp., New York.
30. Fee, J. A., Findling, L., Yoshida, T., Hille, R., Tarr, G. E., Hearshen, D. O., Dunham, W. R., Day, E. P., Kent, T. A., and Munck, E. (1984) *J. Biol. Chem. 259*, 124−133.
31. Degli Esposti, M., Ballester, F., Solaini, G., and Lenaz, G. (1987) *Biochem. J. 241*, 285−290.
32. Link, T. A., Hagen, W. R., Pierik, A. J., Assmann, C., and von Jagow, G. (1992) *Eur. J. Biochem. 208*, 685−691.
33. Prince, R. G., and Dutton, P. L. (1976) *FEBS Lett. 65*, 117−119.
34. Van Doren, S. R., Gennis, R. B., Barquera, B., and Crofts, A. R. (1993) *Biochemistry 32*, 8083−8089.
35. Crofts, A. R., Hong, S., Ugulava, N., Barquera, B., Gennis, R., Guergova-Kuras, M., and Berry, E. A. (1999) *Proc. Natl. Acad. Sci. U.S.A. 96*, 10021−10026.
36. Kuila, D., and Fee, J. A. (1986) *J. Biol. Chem. 261*, 2768−2771.
37. Kuila, D., Schoonover, J. R., Dyer, R. B., Batie, C. J., Ballou, D. P., Fee, J. A., and Woodruff, W. H. (1992) *Biochim. Biophys. Acta 1140*, 175−183.
38. Gatti, D. L., Meinhardt, S. W., Ohnishi, T., and Tzagoloff, A. (1989) *J. Mol. Biol. 205*, 421−435.
39. Liebl, U., Sled, V., Brasseur, G., Ohnishi, T., and Daldal, F. (1997) *Biochemistry 36*, 11675−11684.
40. Crofts, A. R., Berry, E. A., Kuras, R., Guergova-Kuras, M., Hong, S., and Ugulava, N. (1998) in *Photosynthesis: Mechanisms and Effects* (Garab, G., Ed.) Vol. III, pp 1481−1486, Kluwer Academic Publishers, Dordrecht, Boston, and London.
41. Nitschke, W., Joliot, P., Liebl, U., Rutherford, W. A., Hauska, G., Müller, A., and Riedel, A. (1992) *Biochim. Biophys. Acta 1102*, 266−268.
42. Zhang, H., Carrell, C. J., Huang, D., Sled, V., Ohnishi, T., Smith, J. L., and Cramer, W. A. (1996) *J. Biol. Chem. 271*, 31360−31366.
43. Liebl, U., Pezennec, S., Riedel, A., Kellner, E., and Nitschke, W. (1992) *J. Biol. Chem. 267*, 14068−14072.
44. Brugna, M., Albouy, D., and Nitschke, W. (1998) *J. Bacteriol. 180*, 3719−3723.
45. Anemüller, S., Schmidt, C. L., Schafer, G., Bill, E., Trautwein, A. X., and Teixeira, M. (1994) *Biochem. Biophys. Res. Commun. 202*, 252−257.
46. Iwasaki, T., Imai, T., Urushiyama, A., and Oshima, T. (1996) *J. Biol. Chem. 271*, 27659−27663.
47. Brugna, M., Nitschke, W., Asso, M., Guigliarelli, B., Lemesle-Meunier, D., and Schmidt, C. (1999) *J. Biol. Chem. 274*, 16766−16772.
48. DeVault, D. (1980) *Q. Rev. Biophys. 13*, 387−564.
49. Moser, C. C., Page, C. C., Farid, R., and Dutton, P. L. (1995) *J. Bioenerg. Biomembr. 27*, 263−274.
50. Cukier, R. I., and Nocera, D. G. (1998) *Annu. Rev. Phys. Chem. 49*, 337−369.
51. Kim, H., Xia, D., Yu, C. A., Xia, J. Z., Kachurin, A. M., Zhang, L., Yu, L., and Deisenhofer, J. (1998) *Proc. Natl. Acad. Sci. U.S.A. 95*, 8026−8033.
52. Martinez, S. E., Huang, D., Szczepaniak, A., Cramer, W. A., and Smith, J. L. (1994) *Structure 2*, 95−105.
53. Hope, A. B., Valente, P., and Matthews, D. B. (1994) *Photosynth. Res. 42*, 111−120.
54. Nishio, J. N., and Whitmarsh, J. (1993) *Plant Physiol. 101*, 89−96.

BI992491+